iScience

CellPress
OPEN ACCESS

Article

Structural basis of transcription factor YhaJ for DNT detection

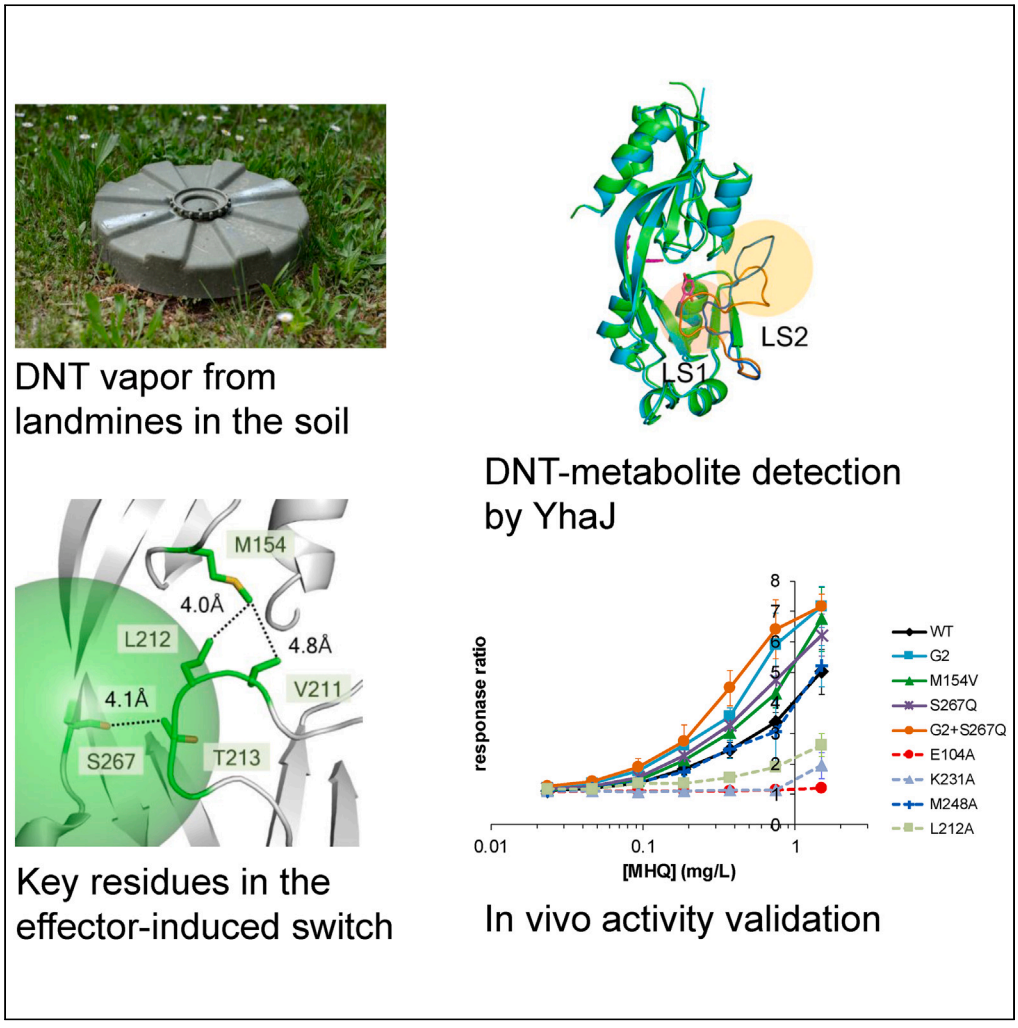

Myeongbin Kim, Ryun Kang, Tae Jin Jeon, Seong Eon Ryu

ryuse@hanyang.ac.kr

Highlights

The bacterial transcription factor YhaJ selectively detects metabolites of explosives

Crystal structures of the apo- and effector-binding forms were determined

The effector-entrance loop significantly switches its conformation

The structures can be used for the rational engineering of sensitive biosensors

Kim et al., iScience 26, 107984
October 20, 2023
https://doi.org/10.1016/j.isci.2023.107984

iScience

CellPress
OPEN ACCESS

Article

Structural basis of transcription factor YhaJ for DNT detection

Myeongbin Kim,[1] Ryun Kang,[1] Tae Jin Jeon,[1,2] and Seong Eon Ryu[1,3,*]

SUMMARY

Detection of landmines without harming personnel is a global issue. The bacterial transcription factor YhaJ selectively detects metabolites of explosives, and it can be used as a key component of DNT biosensors. However, the wild-type YhaJ has a binding affinity that is not sufficient for the detection of trace amounts of explosives leaked from landmines buried in the soil. Here, we report crystal structures of the effector-binding domain of YhaJ in both the apo- and effector-bound forms. A structural comparison of the two forms revealed that the loop above the primary effector-binding site significantly switches its conformation upon effector binding. The primary effector-binding site involves hydrophobic and polar interactions, having specificity to hydroxyl-substituted benzene compounds. The structures explain the mechanism of activity-enhancing mutations and provide information for the rational engineering of YhaJ biosensors for the sensitive detection of explosives.

INTRODUCTION

Landmines are distributed worldwide, causing a major global problem. Despite efforts to eliminate buried landmines, the removal process has been slow because current detection techniques require a direct approach by personnel, triggering dangerous situations. An alternative method to reduce this risk is the application of a bioreporter using genetically engineered microorganisms.[1–4] Cells are modified to harbor components that react with a target chemical and produce a signal, such as luminescence or fluorescence. For landmine detection, bacteria were transformed with engineered plasmid systems responding to vapor from explosives in soil.[3,5,6] These systems respond to 2,4-dinitrotoluene (DNT) which is a volatile and stable impurity in the production of 2,4,6-trinitrotoluene (TNT) explosives.

The LysR-type transcriptional regulator (LTTR) family proteins are transcription factors that are widely distributed in bacteria and are involved in bacteria's metabolism and toxicity.[7] The LTTR family proteins exhibit two functional domains: a DNA-binding domain (DBD) and an effector-binding domain (EBD), which are connected by a single α-helix.[7–10] LTTRs form a homodimer mediated by direct interaction between two EBDs, and two homodimers associate with each other to form a homotetramer.[10] Different modes of tetrameric association lead to different binding modes of LTTRs to the target promoter DNA, enabling transcriptional regulation.[7–10]

YhaJ, a member of the LTTR family, has been shown to detect the metabolic intermediates of explosives.[11,12] Although other LTTRs, such as DntR and NtdR have been exploited for explosives detection, they exhibit a lack of specificity.[13,14] In comparison, YhaJ binds directly to 2,4,5-hydroxtoluene (THT), an intermediate in the DNT metabolic pathway.[11,12] However, current explosives bioreporters utilizing YhaJ require sensitivity-enhancement engineering to overcome its low detection limit.[3,15,16] Although there has been progress in improving YhaJ bioreporters by using directed evolution,[16–19] rational approaches are needed for the development of YhaJ variants that are sensitive enough to detect trace amounts of explosives.

Here, we determined the crystal structures of YhaJ-EBD in both the apo and effector-bound forms. Methylhydroquinone (MHQ), a structural analog of THT, was used as an effector in the structure determination. MHQ induces a YhaJ signal.[12] The structures revealed the mechanism of effector binding, which is mediated by hydrophobic and charged residues in the primary binding pocket located at the interface of the two subdomains of EBD. The effector-bound structure revealed a large conformational switch in the loop that covered the primary binding pocket. Sensitivity-enhancing mutations interact with residues of the switching loop, indicating that loop conformational switches play an important role in effector binding sensitivity. Structural information on YhaJ-effector binding could lead to the rational design and development of highly sensitive and specific YhaJ variants for the detection of explosives.

[1]Department of Bioengineering, College of Engineering, Hanyang University, Seoul 04673, Republic of Korea
[2]National Instrumentation Center for Environmental Management (NICEM), Seoul National University, Seoul 08826, Republic of Korea
[3]Lead contact
*Correspondence: ryuse@hanyang.ac.kr
https://doi.org/10.1016/j.isci.2023.107984

Table 1. Data collection and refinement statistics

	YhaJ-EBD, native	YhaJ-EBD, soaked
Wavelength (Å)	0.9793	0.9793
Space group	H3	H3
Unit cell		
a, b, c (Å)	215.19, 215.19, 263.41	215.75, 215.75, 264.16
α, β, γ (°)	90.00, 90.00, 120.00	90.00, 90.00, 120.00
Resolution range (Å)	36.91–2.64 (2.74–2.64)	35.02–2.80 (2.90–2.80)
Total number of reflections	542435	391535
Unique reflections	131090	107524
Redundancy	4.1	3.6
Completeness (%)	98.2 (94.5)	95.5 (89.9)
I/σI	10.9 (2.6)	10.1 (2.2)
R_{merge}	0.088 (0.386)	0.082 (0.391)
$CC_{1/2}$	0.995 (0.352)	0.996 (0.178)
Reflections used in refinement	124635	101783
Reflections used for R-free	6453	5740
R-work/R-free	0.1771/0.2358	0.1838/0.2320
Number of non-H atoms		
Protein/effector/solvent	25421/15/93	25300/466/71
Number of protein residues	3245	3235
RMS		
Bonds (Å)/angles (°)	0.011/1.75	0.011/1.78
Average B-factors (Å^2)		
Protein/effector/solvent	54.84/40.13/30.18	66.53/69.40/46.44
Ramachandran plot (%)		
Favored/allowed/outliers	95.36/4.33/0.31	94.47/5.00/0.53

RESULTS AND DISCUSSION

Overall structure of YhaJ-EBD

The structure of YhaJ-EBD has a typical fold of LTTRs consisting of six α-helices and eight β-strands that are divided into two subdomains, regulatory domains (RD) 1 (residues 96–168 and 271–298) and 2 (residues 171–268) (Table 1). These subdomains are connected by a hinge region made of antiparallel strands β4 and β8 (Figure 1A). There are eight YhaJ-EBD homodimers (AB, CD, EF, GH, IJ, KL, MN, and OP) in the crystallographic asymmetric unit. The homodimers of YhaJ-EBD adopt a slightly tilted 'head-to-tail' arrangement as previously reported LTTR structures (Figure 1B).[8,10,14,20] The EDB dimers of LTTR's are essential for their *in vivo* function.[7,8] The dimer of YhaJ-EDB exhibits extensive inter-monomer interactions mediated by helix α1 and strand β2 of one monomer with helix α4 and strand β6 of the other monomer (Figure 1B) and the purified YhaJ-EBD is present as a dimer in solution (Figures S1A and S1B). The mutation L223N at the dimeric interface (Figures S1C and S1D) significantly impaired the transcription activity of YhaJ (Figure S1E), supporting the physiological relevance of the dimer. One monomer (A, C, E, G, I, K, M, O) of the dimers has more inter-dimeric crystal contacts than the other monomer (B, D, F, H, J, L, N, and P). Accordingly, we designated the A, C, E, G, I, K, M, and O monomers as the crystal contact-affected (CCA) monomers and the B, D, F, H, J, L, N, and P monomers as the crystal contact-unaffected (CCU) monomers. Because the crystal contacts among the CCA monomers introduced artificial heterogeneity in loop regions, we chose to use the CCU monomers for structure description. For the representative monomer, the B monomer was used.

Superposition of the eight CCU monomers revealed flexibility in two loops including loops β3-β4 (residues 152–161) and β5-β6 (residues 203–221) (Figure 1C). These loop regions are not affected by artificial crystal contacts. These loops are implicated in the effector binding and affinity-enhancing mutations (see below). While the flexibility of loop β3-β4 is restricted to a consistent conformation, regions of loop β5-β6 exhibit different levels of flexibility. Depending on the flexibility level, the β5-β6 loop can be divided into two subregions including loop switch 1 (LS1) and loop switch 2 (LS2) (Figure 1C). The LS1 of eight CCU monomers exhibits a similar conformation. In comparison, two alternate conformations are found in the LS2: three monomers (B, D, and F) in a down position in Figure 1C and five monomers (H, J, L, N, and P)

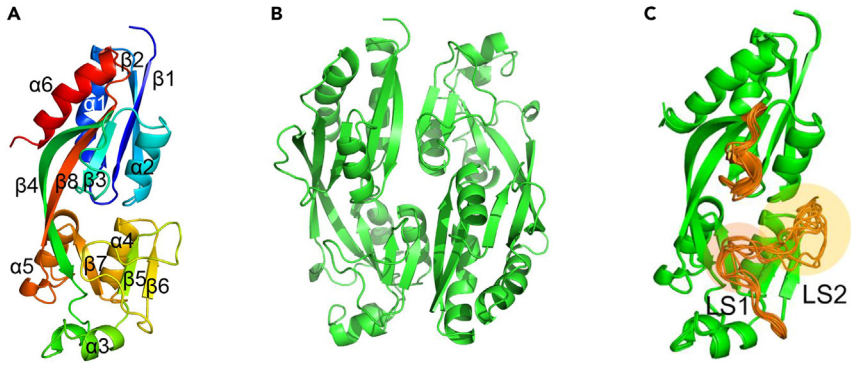

Figure 1. Overall structure

(A) Monomeric structure. The ribbon diagram of YhaJ (B monomer, see text) was presented with secondary structural elements labeled. Boundaries of secondary structures are α1 (T109-K122), α2 (A135-Q143), α3 (E191-K196), α4 (I228-A237), α5 (Y246-E255), α6 (E282-F295), β1 (T97-E104), β2 (T125-E132), β3 (I148-A151), β4 (I162-V175), β5 (G199-V202), β6 (R222-V225), β7 (V241-P245), and β8 (S267-R276).

(B) Dimeric structure. The ribbon diagram of the YhaJ dimer (A and B monomers) was presented. There is a two-fold axis in the center of the dimer.

(C) Comparison of monomers. The ribbon diagrams of the CCU monomers (a total of eight structures) were superimposed. The β3-β4 and β5-β6 loops were colored gold and the β5-β6 loop was highlighted with two circles (LS1 and LS2) to indicate the regions involved in effector-induced loop conformational switches.

in an up position. In the effector-bound state, all eight monomers exhibit an up position in the LS2, indicating that the loop switch is stabilized to the up position by the effector binding (see below).

Effector binding sites

We performed effector-soaking experiments to determine the structure of the effector-bound form of YhaJ-EBD. For the effector-soaking experiments, we used a structural analog of THT, MHQ (Figure 2) which was readily available from the commercial vendor Tokyo Chemical Industry (see STAR Methods). In comparison, THT required custom synthesis. Because both MHQ and THT induced a similar YhaJ signal,[12] we chose MHQ for the effector soaking experiments. In the structure of the effector-soaked YhaJ-EBD, we found three effector binding sites (S1-S3), where S1 and S2 are strong binding sites with prominent binding pockets and S3 is a weak binding site in the molecular surface (Figure 3). The MHQ molecule is found in S1-S3 of all 16 monomers in the asymmetric unit. S1 resides in a deep pocket at the center of YhaJ-EBD made with residues of loops β1-α1 and β2-α3 and strands β5 and β7 (Figure 3). The pocket entrance for S1 is covered by residues of loops β3-β4 and β5-β6 in the apo state, while the entrance is open in the soaked state due to conformational switches (see below).

S2 resides in a relatively shallow pocket formed by residues of helices α2 and α5 and strand β4 (Figure 3). S2 is often on the molecular surface. Although both S1 and S2 are in the interface of RD1 and RD2, there is no direct contact between effectors in the two sites. The MHQ molecule in S3 is tethered to the MHQ molecule in S2 (Figure 3). Thus, S3 is likely not a physiological binding site. The location of S1 is close to the primary effector binding sites of other LTTRs including BenM, PqsR, OccR, CysB, and LysG,[21–25] suggesting that S1 is the primary effector binding site in YhaJ-EBD. Interestingly, despite the similarity of the overall location of the primary effector binding sites of YhaJ-EBD and other LTTRs, the actual location and EBD interactions of effectors exhibit significant variation, reflecting the evolution of LTTR's for divergent effector binding (data not shown).

Effector-induced conformational switch

Upon effector binding, the loop β5-β6 covering S1 undergoes a large conformational switch, opening the entrance to the pocket (Figure 4). Other sites do not exhibit structural differences between the apo and effector-bound forms. In Figures 4A and 4B, we aligned the apo and effector-bound structures. In the apo structures, the LS1 of the β5-β6 loop forms interactions with regions of the central β-sheet including strand β8, strand β4, and strand β7. The LS1 also interacts with the β3-β4 loop including Met154 which was implicated in the sensitivity-enhancing mutagenesis studies (Figure 4C)[16,19] (see below). Upon effector binding, the LS1 moves away from the cavity (Figures 4A, 4B, and 4D), which is seen in all eight CCU monomers. The LS1 movement broadens the entrance area of S1, facilitating the approach of an effector to the binding site. The LS1 movement appears to induce stabilization of the LS2 in an up position in all eight CCU monomers (Figure 4B).[26]

Recent studies on the engineering of YhaJ bioreporters have shown an important role of the β3-β4 loop in effector detection sensitivity.[16,19] Elad et al. performed directed evolution on YhaJ protein to find mutations that yielded improved effector-sensing sensitivity. They found that the M154T mutation in the β3-β4 loop improved the sensitivity in all generations of screening.[16] Interestingly, an independent study by Zhang et al. also found that the M154V mutation was a common mutation site that appeared in 864 sensitivity-enhanced transformants, indicating that the residue plays an important role in the effector-sensing process.[19] In the YhaJ-EBD structures, the side chain of Met154 makes hydrophobic interactions with residues of the LS1 in loop β5-β6 holding the loop in a closed conformation (Figure 4C). The mutations on Met154 to smaller amino acids break these interactions, increasing the chance of loop opening for effector binding.

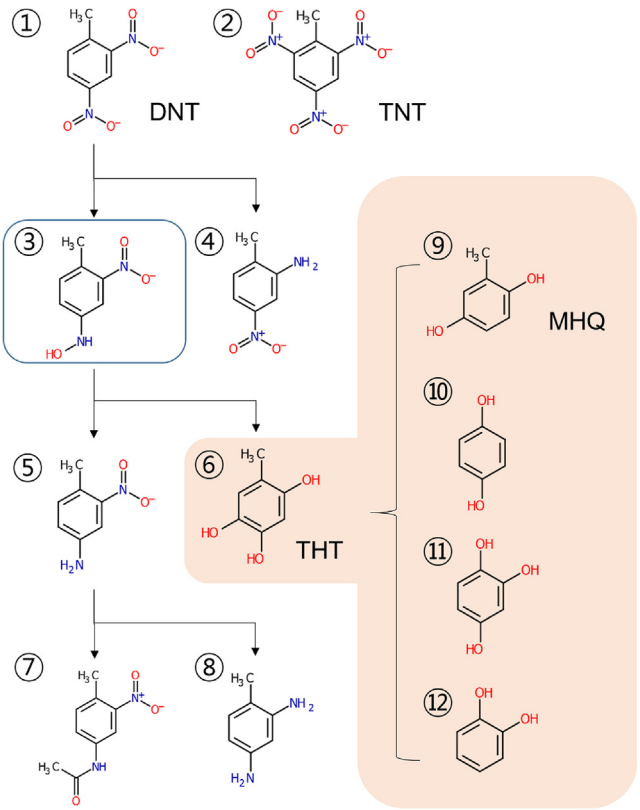

Figure 2. Effector structures

Metabolic intermediates of trinitrotoluene and dinitrotoluene are presented: ① dinitrotoluene; ② trinitrotoluene; ③ 4-hydroxylamino-2-nitrotoluene; ④ 2-amino-4-nitrotoluene; ⑤ 4-methyl-3-nitroaniline; ⑥ 2,4,5-trihydroxytoluene; ⑦ 4-acetamide-2-nitrotolene; ⑧ 2,4-diaminotoluene; ⑨ methylhydroquinone; ⑩ hydroxyquinone; ⑪ 1,2,4-benzenetriol; ⑫ catechol. Among the intermediates, those exhibiting immediate and strong transcription responses[12] are colored peach. Intermediate 3 showed a lagged and strong response (Figure 4 of Henshke et al.[12]).

The region corresponding to loop β5-β6 participates in the tetrameric interaction of other LTTR's including CbnR[10] and OxyR.[8] The tetramer is a functional unit of LTTR's in the transcription activation and the switch in the tetrameric association mode is critical for the differential binding to the target promotor.[10] Thus, the effector-induced switch of the loop β5-β6 conformation would lead to the switch of the tetrameric association mode, resulting in the modulation of transcription activation. In CbnR, the tetrameric association in the crystal structure of the full-length protein was mediated by the region corresponding to the β5-β6 loop of YhaJ.[10] In OxyR, the conformational change by oxidation of the corresponding loop was observed, suggesting that the loop plays a role in the tetrameric association and redox-regulated transcription switches.[8] Tetrameric association and transcription regulation of LTTRs are also thought to be regulated by the interdomain movement between RD1 and RD2.[21] YhaJ-EBD also exhibits interdomain movement (Figure S2A). However, the extent of domain movement is relatively smaller compared to other LTTRs. When RD1 was aligned between the apo and effector-bond forms of YhaJ, the movement distance of RD1 was about 1 Å (Figure S2A), while the corresponding movement distance of DntR is over 6 Å (Figure S2B). Interestingly, the region corresponding to the YhaJ-EBD β5-β6 loop does not exhibit structural switches between the apo and effector-bound structures of many LTTRs. Thus, YhaJ seems to have a unique mechanism of transcription regulation that involves both the interdomain movement and the β5-β6 loop conformational switch.

Specificity determinants

Binding of MHQ to the primary site is stabilized by hydrophobic interactions with Leu106, Val133, Leu134, and Val202, and hydrogen bonds of two hydroxyl groups of MHQ with Glu104 and Lys231 (Figures 5A and 5B). The hydrogen bond distances with O-O and N-O interactions are 3.1 Å and 2.8 Å, respectively (Figures 5A and 5B). Previous studies reported that THT and its structural analogs induced an immediate response of the YhaJ sensor, whereas other metabolic intermediates of DNT caused no or lagged signal.[12] In particular, aromatic rings with two hydroxyl or ketone groups induced a clear signal[11,12] (Figure 2), consistent with structural observations. These hydroxyl or ketone groups can form hydrogen bond interactions with side chains of Glu104 and Lys231 that are located at opposing ends of the binding pocket. Bulky groups in TNT and DNT-derived intermediates appear to result in clashes with side chains in the primary binding pocket. Interestingly, one exception exists in the interpretation. One of the DNT-derived intermediates, 4-hydroxylamino-2-nitrotoluene (numbered as 3 in Figure 2)

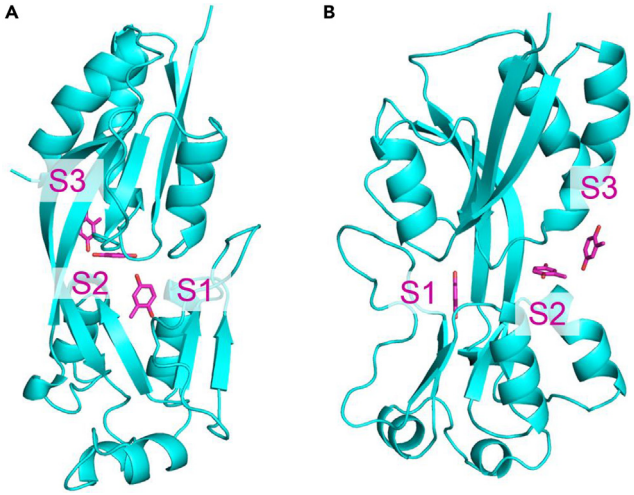

Figure 3. Effector binding sites

(A and B) The effector-soaked structure of YhaJ-EBD was presented. The bound MHQ molecules were shown with the three effector binding sites (S1-S3) labeled. The orientation of (A) is the same as in Figure 1 and that of (B) is about 90° rotation of (A).

with a bulky nitro-substitution in the toluene ring exhibited a relatively strong response with a lagging period.[12] This exception can be explained by two possible mechanisms: flexibility of binding interactions in S1 or the usage of S2 (see below).

In the effector-bound YhaJ structure, the MHQ molecule in S2 makes van der Waals interactions with side chains of Pro108 and Met248 having interaction distances of 3–4 Å (Figure 5C). Although other residues forming the binding pocket surround the molecule, the interaction distances are over 4.5 Å, indicating that the binding interactions are weak. There are no hydrogen bond interactions with the two hydroxyl groups of MHQ. Two interpretations would be possible for the loose interactions in S2. First, the MHQ molecule binding to S2 may be an artifact due to crystal conditions. Second, the S2 site may favor different effectors (see below). The Hill coefficient of the wild-type YhaJ-EBD was 1.25 (Figure S3), indicating small cooperativity. The cooperativity may arise from both the dimeric state of YhaJ-EBD and the S2 binding. We could not find an indication for the secondary binding transition until 100 mM of MHQ (data not shown), indicating a very low binding affinity of S2. In addition, the M248A mutation in the S2 site did not change the *in vivo* activity (Figure 6). Thus, the contribution of the S2 site to the cooperativity is likely minimal. Because the binding affinity of S2 appears to be very low, S2 may favor different effectors as shown in BenM that bound to two different effectors in two binding sites (Craven, Ezezika et al. 2009). S2 can bind to an alternative effector with bulky groups in the toluene ring. For example, the lagged response inducer 4-hydroxylamino-2-nitrotoluene may favor binding to S2. Further biochemical and functional analyses using combinations of different effectors are needed for an explanation of the effector specificity and the role of S2 in the transcription regulation of YhaJ.

In vitro and *in vivo* analysis of effector binding

The effector binding affinity of YhaJ wild-type and mutants was analyzed by determining the dissociation constant between YhaJ and the effector (Table 2). The wild-type YhaJ exhibited a dissociation constant (Kd) of 11.0 mM, whereas the residues involved in the effector-induced conformational switch and the effector binding site affected the binding constant. The activity-enhancing M154V mutation[19] exhibited a decreased Kd of 8.4 mM (affinity increased). Based on the structural information, we screened residues that would have potential roles in the effector binding. The L212A mutation that would destabilize interactions of loop β5-β6 with Met 154 decreased Kd to 9.0 mM, confirming the role of loop β5-β6 in the effector binding. From the structures, we predicted that the S267Q mutation in strand β8 would destabilize the left-hand side of loop β5-β6 by introducing steric hindrance between Q267 and loop β5-β6 (Figure 4C). The Kd of S267Q also decreased to 8.4 mM, confirming the structural prediction. In comparison to the mutations promoting the loop switch, mutations in the residues making direct effector interactions in the binding pocket significantly increased the dissociation constant (affinity decreased). The charged residues Glu 104 and Lys 231 in the effector-binding pocket S1 contribute polar interactions to the hydroxyl groups of MHQ (Figure 5B). E104A and K231A exhibited increased Kd's of 18.9 and 28.5 mM, respectively.

The *in vivo* activity of YhaJ mutants was analyzed by estimating the transcription level of a reporter protein placed downstream of the target promoter (Figures 6 and S4). The S267Q mutant, which would destabilize loop β5-β6 (Figure 4C), exhibited a comparable *in vivo* activity increase to the previously found M154V mutant, confirming the role of loop β5-β6 in the effector binding. The addition of S267Q to the previously reported G2 (M154T + A274V + a DNA-binding site mutant) resulted in stronger transactivation than G2. Unlike S267Q in strand β8, the other loop-destabilizing mutation L212A in loop β5-β6 decreased the transcription activity even though it increased the effector binding affinity (Table 2). The dual effect of L212A is likely because loop β5-β6 plays a role in the tetramer formation for transcription activation. Only the mutations of the residues not involved in the tetrameric interaction appear to have the potential for enhancing transcription activation. The E104A and K231A mutations in the effector-binding pocket (Figures 5A and 5B) disrupted the

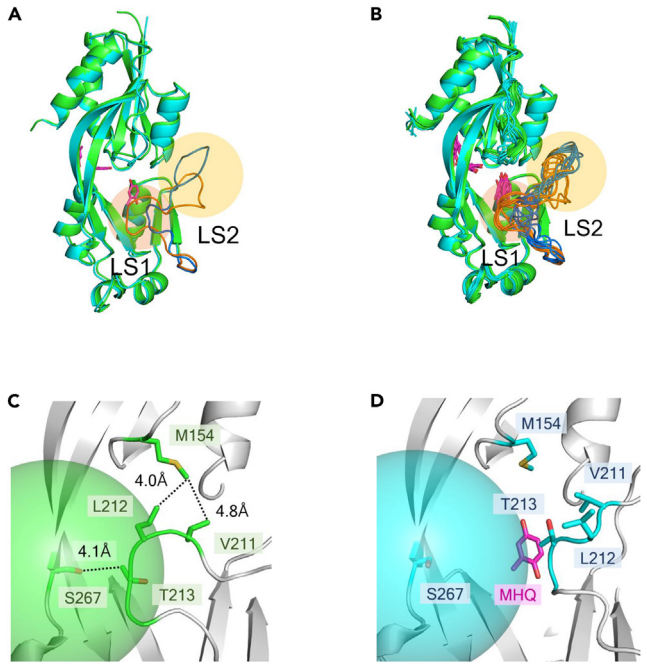

Figure 4. Conformational switch in the primary effector binding site S1

(A) and (B) Superposition of the apo and effector-bound structures. The apo (cyan) and effector-bound (green) structures of B monomer (A) and all CCU monomers (B) were superimposed. The β5-β6 loop was colored differently: gold for the apo and blue for the effector-bound structures. The regions of structural switches (LS1 and LS2) were circled and labeled. The effector molecules (MHQ) were colored purple.

(C) The close-up view of the loops covering the S1-site in the apo structure of monomer B. Interactions of Val 211, Leu 212, and Thr 213 in loop β5-β6 with Met 154 in loop β3-β4 and Ser 267 in strand β8 are shown. The green sphere with a radius of 6.0 Å represents the length of the Gln side chain introduced in the S267Q mutant.

(D) The close-up view of the region as in (C) in the effector-bound structure of monomer B. Val 211, Leu 212, and Thr 213 are far away from Met 154 and Ser 267 due to the conformational switch in loop β5-β6. The S267Q sphere is in cyan.

transcription activity, consistent with the structural prediction and the binding affinity decrease (Table 2). The M248A mutant in the S2 site (Figure 5C) did not affect the *in vivo* activity. Extensive structure-based mutations of different combinations in the structural-switch region and the effector-binding pocket would facilitate the optimization of biosensors for sensitive and specific detection of explosives.

Conclusions

Crystal structures of the apo and effector-bound YhaJ-EBD revealed that the loop covering the primary effector-binding site significantly switches its conformation upon effector binding. In comparison to other LTTRs, the effector-induced loop conformational switch is unique

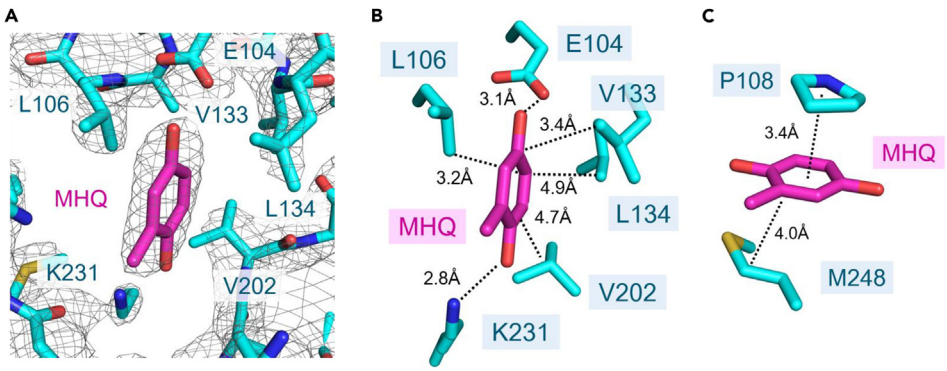

Figure 5. Specific interactions in the binding pockets

(A) Electron density of the S1 region. The S1 region of the effector-bound structure was shown with an electron density map (2Fo-Fc, 1.2σ). The effector MHQ and interacting side chains were labeled.

(B and C) Interactions in the S1 and S2 regions. The interactions between MHQ and the interacting side chains in S1 (B) and S2 (C) were shown with broken lines and interacting distances.

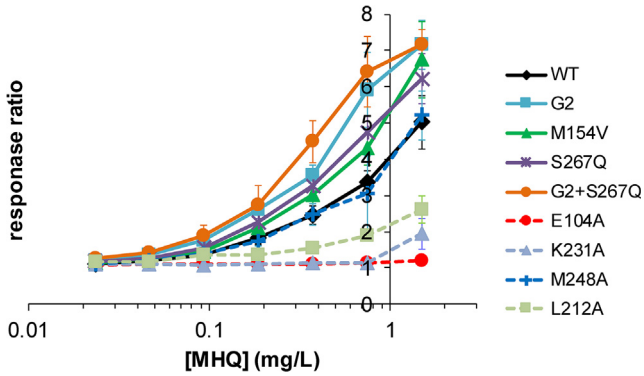

Figure 6. *In vivo* activity

The *in vivo* activities of YhaJ mutants are presented. X and Y axes are the concentration of MHQ in the log scale and the response ratio (see STAR Methods), respectively. The line type and color of wild type (WT) and mutants (G2, M154V, S267Q, G2 + S267Q, E104A, K231A, M248A, and L212A) are indicated on the right-hand side of the graph. The G2 mutant[16] is the combination of M154T + A274V together with a DNA-binding domain mutation.

to YhaJ and explains the mechanism of sensitivity-enhancing mutations. In addition, the loop with a conformational switch corresponds to the region that was shown to be involved in tetrameric interactions in other LTTRs, indicating that the loop conformational switch has a role in the transcriptional regulation of target genes. The bound effector MHQ made strong hydrophobic interactions and characteristic hydrogen bonds with residues of YhaJ, explaining the specificity of YhaJ to a special group of metabolic intermediates of DNT containing hydroxyl or ketone substitutions in the benzene ring. The *in vitro* and *in vivo* analysis of mutants involved in the loop-structural switch and the effector-binding pocket confirmed the structure-based interpretation of the YhaJ transactivation by MHQ. Structural information can lead to the rational design of biosensors for explosives with optimized sensitivity and specificity.

Limitation of the study

This study presents the EBD structures of YhaJ. Because the transcription activity of YhaJ is affected by both the EBD and the DBD, the comprehensive understanding of the transcription mechanism and the more sensitive biosensor design would await structural and biochemical studies of the DBD and the full-length protein containing both domains.

STAR★METHODS

Detailed methods are provided in the online version of this paper and include the following:

- KEY RESOURCES TABLE
- RESOURCE AVAILABILITY
  - Lead contact
  - Materials availability
  - Data and code availability
- EXPERIMENTAL MODEL AND SUBJECT DETAILS
- METHOD DETAILS
  - Cloning and expression
  - Crystallization
  - Structure determination
  - Microscale thermophoresis assay
  - GFP-based *in vivo* activity assay

Table 2. Dissociation constants for MHQ

YhaJ-EBD	Kd (mM)	Fold change
WT	11.0 ± 3.7	1.00
M154V	8.4 ± 2.4	0.76
L212A	9.0 ± 3.7	0.82
S267Q	8.4 ± 2.2	0.76
E104A	18.9 ± 5.3	1.72
K231A	28.5 ± 5.4	2.59

- QUANTIFICATION AND STATISTICAL ANALYSIS
  - Crystallography
  - Microscale thermophoresis assay
  - GFP-based *in vivo* activity assay

SUPPLEMENTAL INFORMATION

Supplemental information can be found online at https://doi.org/10.1016/j.isci.2023.107984.

ACKNOWLEDGMENTS

We thank the staff members of beamline 7A at the Pohang Accelerator Laboratory (PAL) for diffraction data collection. This work was funded by the biomedical technology development project, National Research Foundation, Korea [NRF-2015M3A9B5030302 and 2021M3A 9G8024747].

AUTHOR CONTRIBUTIONS

Conceptualization: M.K. and S.E.R. Methodology: M.K., R.K., T.J.J., and S.E.R. Investigation: M.K., R.K., T.J.J., and S.E.R. Supervision: S.E.R. Writing – Original Draft: M.K. and S.E.R. Writing – Review and Editing: M.K., R.K., T.J.J., and S.E.R.

DECLARATION OF INTERESTS

The authors declare no competing interests.

INCLUSION AND DIVERSITY

We support inclusive, diverse, and equitable conduct of research.

Received: October 25, 2022
Revised: July 11, 2023
Accepted: September 16, 2023
Published: September 21, 2023

REFERENCES

1. Meyer, A.J., Segall-Shapiro, T.H., Glassey, E., Zhang, J., and Voigt, C.A. (2019). Escherichia coli "Marionette" strains with 12 highly optimized small-molecule sensors. Nat. Chem. Biol. *15*, 196–204. https://doi.org/10.1038/s41589-018-0168-3.
2. Kabessa, Y., Eyal, O., Bar-On, O., Korouma, V., Yagur-Kroll, S., Belkin, S., and Agranat, A.J. (2016). Standoff detection of explosives and buried landmines using fluorescent bacterial sensor cells. Biosens. Bioelectron. *79*, 784–788. https://doi.org/10.1016/j.bios.2016.01.011.
3. Shemer, B., Koshet, O., Yagur-Kroll, S., and Belkin, S. (2017). Microbial bioreporters of trace explosives. Curr. Opin. Biotechnol. *45*, 113–119. https://doi.org/10.1016/j.copbio.2017.03.003.
4. Alhadrami, H.A. (2018). Biosensors: Classifications, medical applications, and future prospective. Biotechnol. Appl. Biochem. *65*, 497–508. https://doi.org/10.1002/bab.1621.
5. Yagur-Kroll, S., Amiel, E., Rosen, R., and Belkin, S. (2015). Detection of 2,4-dinitrotoluene and 2,4,6-trinitrotoluene by an Escherichia coli bioreporter: performance enhancement by directed evolution. Appl. Microbiol. Biotechnol. *99*, 7177–7188. https://doi.org/10.1007/s00253-015-6607-0.
6. Palevsky, N., Shemer, B., Connolly, J.P.R., and Belkin, S. (2016). The Highly Conserved Escherichia coli Transcription Factor YhaJ Regulates Aromatic Compound Degradation. Front. Microbiol. *7*, 1490. https://doi.org/10.3389/fmicb.2016.01490.
7. Maddocks, S.E., and Oyston, P.C.F. (2008). Structure and function of the LysR-type transcriptional regulator (LTTR) family proteins. Microbiology (Read.) *154*, 3609–3623. https://doi.org/10.1099/mic.0.2008/022772-0.
8. Choi, H., Kim, S., Mukhopadhyay, P., Cho, S., Woo, J., Storz, G., and Ryu, S.E. (2001). Structural basis of the redox switch in the OxyR transcription factor. Cell *105*, 103–113. https://doi.org/10.1016/s0092-8674(01)00300-2.
9. Hong, S., Kim, J., Cho, E., Na, S., Yoo, Y.J., Cho, Y.H., Ryu, S., and Ha, N.C. (2022). Crystal structures of YeiE from Cronobacter sakazakii and the role of sulfite tolerance in gram-negative bacteria. Proc. Natl. Acad. Sci. USA *119*. e2118002119. https://doi.org/10.1073/pnas.2118002119.
10. Giannopoulou, E.A., Senda, M., Koentjoro, M.P., Adachi, N., Ogawa, N., and Senda, T. (2021). Crystal structure of the full-length LysR-type transcription regulator CbnR in complex with promoter DNA. FEBS J. *288*, 4560–4575. https://doi.org/10.1111/febs.15764.
11. Shemer, B., Yagur-Kroll, S., Hazan, C., and Belkin, S. (2018). Aerobic Transformation of 2,4-Dinitrotoluene by Escherichia coli and Its Implications for the Detection of Trace Explosives. Appl. Environ. Microbiol. *84*, e01729-17. https://doi.org/10.1128/AEM.01729-17.
12. Henshke, Y., Shemer, B., and Belkin, S. (2021). The Escherichia coli azoR gene promoter: A new sensing element for microbial biodetection of trace explosives. Curr. Res. Biotechnol. *3*, 21–28.
13. Ju, K.S., Parales, J.V., and Parales, R.E. (2009). Reconstructing the evolutionary history of nitrotoluene detection in the transcriptional regulator NtdR. Mol. Microbiol. *74*, 826–843. https://doi.org/10.1111/j.1365-2958.2009.06904.x.
14. Smirnova, I.A., Dian, C., Leonard, G.A., McSweeney, S., Birse, D., and Brzezinski, P. (2004). Development of a bacterial biosensor for nitrotoluenes: the crystal structure of the transcriptional regulator DntR. J. Mol. Biol. *340*, 405–418. https://doi.org/10.1016/j.jmb.2004.04.071.
15. Jenkins, T.F., Leggett, D.C., Miyares, P.H., Walsh, M.E., Ranney, T.A., Cragin, J.H., and George, V. (2001). Chemical signatures of TNT-filled land mines. Talanta *54*, 501–513. https://doi.org/10.1016/s0039-9140(00)00547-6.
16. Elad, T., Shemer, B., Simanowitz, S., Kabessa, Y., Mizrachi, Y., Gold, A., Shpigel, E., Agranat, A.J., and Belkin, S. (2022). Enhancing DNT Detection by a Bacterial Bioreporter: Directed Evolution of the Transcriptional Activator YhaJ. Front. Bioeng. Biotechnol. *10*, 821835. https://doi.org/10.3389/fbioe.2022.821835.
17. Shemer, B., Shpigel, E., Glozman, A., Yagur-Kroll, S., Kabessa, Y., Agranat, A.J., and Belkin, S. (2020). Genome-wide

gene-deletion screening identifies mutations that significantly enhance explosives vapor detection by a microbial sensor. N. Biotechnol. *59*, 65–73. https://doi.org/10.1016/j.nbt.2020.06.002.

18. Shpigel, E., Shemer, B., Elad, T., Glozman, A., and Belkin, S. (2021). Bacterial bioreporters for the detection of trace explosives: performance enhancement by DNA shuffling and random mutagenesis. Appl. Microbiol. Biotechnol. *105*, 4329–4337. https://doi.org/10.1007/s00253-021-11290-2.
19. Zhang, Y., Zou, Z.P., Chen, S.Y., Wei, W.P., Zhou, Y., and Ye, B.C. (2022). Design and optimization of E. coli artificial genetic circuits for detection of explosive composition 2,4-dinitrotoluene. Biosens. Bioelectron. *207*, 114205. https://doi.org/10.1016/j.bios.2022.114205.
20. Devesse, L., Smirnova, I., Lönneborg, R., Kapp, U., Brzezinski, P., Leonard, G.A., and Dian, C. (2011). Crystal structures of DntR inducer binding domains in complex with salicylate offer insights into the activation of LysR-type transcriptional regulators. Mol. Microbiol. *81*, 354–367. https://doi.org/10.1111/j.1365-2958.2011.07673.x.
21. Ezezika, O.C., Haddad, S., Clark, T.J., Neidle, E.L., and Momany, C. (2007). Distinct effector-binding sites enable synergistic transcriptional activation by BenM, a LysR-type regulator. J. Mol. Biol. *367*, 616–629. https://doi.org/10.1016/j.jmb.2006.09.090.
22. Ilangovan, A., Fletcher, M., Rampioni, G., Pustelny, C., Rumbaugh, K., Heeb, S., Cámara, M., Truman, A., Chhabra, S.R., Emsley, J., and Williams, P. (2013). Structural basis for native agonist and synthetic inhibitor recognition by the Pseudomonas aeruginosa quorum sensing regulator PqsR (MvfR). PLoS Pathog. *9*, e1003508. https://doi.org/10.1371/journal.ppat.1003508.
23. Kim, Y., Chhor, G., Tsai, C.S., Winans, J.B., Jedrzejczak, R., Joachimiak, A., and Winans, S.C. (2018). Crystal structure of the ligand-binding domain of a LysR-type transcriptional regulator: transcriptional activation via a rotary switch. Mol. Microbiol. *110*, 550–561. https://doi.org/10.1111/mmi.14115.
24. Mittal, M., Singh, A.K., and Kumaran, S. (2017). Structural and biochemical characterization of ligand recognition by CysB, the master regulator of sulfate metabolism. Biochimie *142*, 112–124. https://doi.org/10.1016/j.biochi.2017.08.011.
25. Della Corte, D., van Beek, H.L., Syberg, F., Schallmey, M., Tobola, F., Cormann, K.U., Schlicker, C., Baumann, P.T., Krumbach, K., Sokolowsky, S., et al. (2020). Engineering and application of a biosensor with focused ligand specificity. Nat. Commun. *11*, 4851. https://doi.org/10.1038/s41467-020-18400-0.
26. Emsley, P., and Cowtan, K. (2004). Coot: model-building tools for molecular graphics. Acta Crystallogr. D Biol. Crystallogr. *60*, 2126–2132. https://doi.org/10.1107/S0907444904019158.
27. Otwinowski, Z., and Minor, W. (1997). Processing of X-ray diffraction data collected in oscillation mode. Methods Enzymol.. Elsevier.
28. Zwart, P.H., Afonine, P.V., Grosse-Kunstleve, R.W., Hung, L.W., Ioerger, T.R., McCoy, A.J., McKee, E., Moriarty, N.W., Read, R.J., Sacchettini, J.C., et al. (2008). Automated structure solution with the PHENIX suite. Methods Mol. Biol. *426*, 419–435. https://doi.org/10.1007/978-1-60327-058-8_28.
29. Murshudov, G.N., Vagin, A.A., and Dodson, E.J. (1997). Refinement of macromolecular structures by the maximum-likelihood method. Acta Crystallogr. D Biol. Crystallogr. *53*, 240–255. https://doi.org/10.1107/S0907444996012255.
30. McCoy, A.J. (2007). Solving structures of protein complexes by molecular replacement with Phaser. Acta Crystallogr. D Biol. Crystallogr. *63*, 32–41. https://doi.org/10.1107/S0907444906045975.
31. Yagur-Kroll, S., Lalush, C., Rosen, R., Bachar, N., Moskovitz, Y., and Belkin, S. (2014). Escherichia coli bioreporters for the detection of 2,4-dinitrotoluene and 2,4,6-trinitrotoluene. Appl. Microbiol. Biotechnol. *98*, 885–895. https://doi.org/10.1007/s00253-013-4888-8.

STAR★METHODS

KEY RESOURCES TABLE

REAGENT or RESOURCE	SOURCE	IDENTIFIER
Bacterial and virus strains		
DH5α Chemically Competent *E. coli*	Enzynomics	Cat# CP010
BL21(DE3) Chemically Competent *E. coli*	Enzynomics	Cat# CP110
One Shot™ TOP10 Chemically Competent *E. coli*	Invitrogen	Cat# C404010
Chemicals, peptides, and recombinant proteins		
Methylhydroquinone	Tokyo Chemical Industry	Cat# M0342
Ni-nitrilotriacetate resin	Qiagen	Cat# 30210
HiPrep 16/60 Sephacryl S-100 HR	Cytiva	Cat# 17116501
Monolith His-Tag Labeling Kit RED-tris-NTA	NanoTemper Technologies	Cat# MO-L018
Monolith NT.115 Capillaries	NanoTemper Technologies	Cat# MO-K022
Deposited data		
Crystal structure of YhaJ effector binding domain	This paper	PDB ID 8H58
Crystal structure of YhaJ effector binding domain (ligand-bound)	This paper	PDB ID 8H5A
Recombinant DNA		
pET28a-YhaJ-EBD	This paper	N/A
pETDuet-1-c55-GFPmut2-YhaJ	This paper	N/A
Software and algorithms		
HKL-2000	Otwinowski and Minor[27]	https://hkl-xray.com/hkl-2000
Phenix	Zwart et al.[28]	https://phenix-online.org/
CCP4	Murshudov et al.[29]	https://legacy.ccp4.ac.uk
Coot	Emsley and Cowtan[26]	https://www2.mrc-lmb.cam.ac.uk/personal/pemsley/coot/
MO.Affinity Analysis	NanoTemper Technologies	https://nanotempertech.com/monolith/

RESOURCE AVAILABILITY

Lead contact

Further information and requests for resources should be directed to and will be fulfilled by the corresponding author, Seong Eon Ryu (ryuse@hanyang.ac.kr).

Materials availability

This study did not generate any new materials or reagents.

Data and code availability

- The coordinates for the apo and effector-bound forms have been deposited in the Protein Data Bank under the accession codes 8H58 and 8H5A, respectively. The Protein Data Bank data sets are publicly accessible. All other original data reported in this paper will be shared by the lead contact upon request.
- This paper does not report original codes.
- Any additional information required to reanalyze the data reported in the paper is available from the lead contact upon request.

EXPERIMENTAL MODEL AND SUBJECT DETAILS

This study did not involve human or animal models.

METHOD DETAILS

Cloning and expression

The gene encoding *E. coli* transcription factor YhaJ (Uniprot P67660-1) was obtained from the lysate of *E. coli* DH5α by polymerase chain reaction (PCR) using primers 5′-ATGGCCAAAGAAAGGGCA-3′ and 5′-TTTTCCGTTAAAAAGTTTGGGA-3′. The gene fragment for EBD of YhaJ (residues 96-298) was PCR-amplified by using this full-length YhaJ gene as a template. The restriction enzyme recognition sites for NdeI and HindIII were added to the gene. The PCR product and the plasmid vector pET-28a were digested by restriction enzymes (New England Biolabs) at 37°C and ligated by T4 DNA ligase (Enzynomics) at 16°C overnight. DNA sequences were confirmed by a sequencing service (Bionics).

The protein was expressed in *E. coli* BL21(DE3). The cells transformed with the plasmid DNA encoding YhaJ were cultured in LB medium supplemented with 30 μg/mL kanamycin at 37°C, until OD600 reached about 0.6. To induce the overexpression of the protein, a final concentration of 0.1 mM isopropyl β-D-1-thiogalactopyranoside was added to the culture. The cells were further incubated at 18°C overnight and harvested by centrifugation. After resuspension in lysis buffer (40 mM Tris-Cl pH 7.5, 0.5 M NaCl, 5% glycerol, and 5 mM 2-mercaptoethanol), cells were disrupted by sonication. The soluble fraction of the lysate was obtained by centrifugation at 4°C for an hour. The supernatant derived from centrifugation was loaded onto the affinity chromatography column containing nickel nitrilotriacetic acid resin. Then, the resin was washed with 40 mM Tris-Cl pH 7.5, and 0.5 M NaCl. The imidazole-containing buffer (40 mM Tris-Cl pH 7.5, 0.2 M NaCl, 0.5 M imidazole, and 5 mM 2-mercaptoethanol) was applied to the column to elute the YhaJ protein. The fractions were pooled, and thrombin was added to remove the N-terminal tag for nickel affinity chromatography. YhaJ was further purified by Sephacryl S-100 gel filtration chromatography column (Cytiva) equilibrated with a buffer (20 mM Tris-Cl pH 7.5, 150 mM NaCl, and 2 mM dithiothreitol). The eluted protein was concentrated to 30 mg/mL and stored at -70°C.

Crystallization

The initial screening was conducted using commercially available crystallization kits using a sitting-drop vapor-diffusion method at 18°C. Crystals appeared within 2 days in a mixture of equal volumes of protein solution and reservoir buffer (0.5 M sodium formate pH 7.0 and 4 M sodium chloride), equilibrated with 70 μL of reservoir buffer in a 96-well plate. However, initial crystals had a pathologic property hindering molecular replacement (MR) calculation, which resulted in high R-free values. The interpretable crystals were obtained from random microseed matrix screenings. The reservoir solution of 2.8 M sodium acetate trihydrate pH 7.0 produced bipyramid-shaped crystals utilized in the determination of apo and effector-bound structures. For effector soaking, crystals were transferred to a soaking solution (2.8 M sodium acetate trihydrate pH 7.0, 10 mM dithiothreitol, and 10 mM MHQ (Tokyo Chemical Industry)) a half-day before diffraction data collection. To prevent precipitation by oxidation, 10 mM dithiothreitol was added to the soaking solution.

Structure determination

Diffraction datasets were obtained at synchrotron beamline 7A in Pohang Accelerator Laboratory. Prior to diffraction, crystals were briefly soaked to cryo-protectant solution (2.8 M sodium acetate trihydrate and 15% glycerol for the apo crystal; 2.8 M sodium acetate trihydrate, 15% glycerol, 10 mM dithiothreitol and 5 mM MHQ for the effector-soaked crystal). The data were processed using HKL-2000.[27] The valid molecular MR solution was found by Phaser[30] using a model obtained from the AlphaFold database (residues 96-298; AF-P67660-F1-model_v1) as an initial search model. The MHQ-soaked structure was solved by MR using the apo structure as a search model. The MR software placed 16 molecules in the asymmetric unit as 8 homodimers. Each molecule in the asymmetric unit showed high structural similarity, except for flexible loops (see Results). The resulting structure was manually modified and refined by the Coot and Refmac5 in the CCP4 suite.[26,29] Because Refmac5 found twin operators from the data, the iterative refinement steps were conducted under the twin refinement option. Ligand modeling was conducted by using the eLBOW, Ligand Fit, and ReadySet in the Phenix suite[28] and the Coot. The statistics for the data collection and refinement are presented in Table 1.

Microscale thermophoresis assay

The binding affinity between YhaJ-EBD and MHQ was measured using Monolith NT.115 pico (NanoTemper Technologies). Before protein labeling, purified YhaJ-EBD proteins were buffer-exchanged into a labeling-compatible buffer (20 mM HEPES-NaOH pH 7.5, 150 mM NaCl, and 2 M dithiothreitol). The proteins were stained using Monolith His-Tag Labeling Kit RED-tris-NTA (NanoTemper Technologies) according to the manufacturer's protocol, as diluted in PBST pH 7.5 buffer with 0.05% Tween-20 and 2 mM dithiothreitol. MHQ was prepared in the same buffer with 12 serially-diluted concentrations. YhaJ-EBD proteins of the final concentration of 20 nM and MHQ were mixed and loaded to Monolith NT.115 Capillaries (NanoTemper Technologies). Measurements were conducted under 20% excitation power, and MST power at medium option. The data were analyzed using the MO.Affinity Analysis software (NanoTemper Technologies). The Hill coefficients were calculated using OriginPro (OriginLab).

GFP-based *in vivo* activity assay

The *yhaJ* gene and the modified *yqjF* promoter C55[16] linked to the GFPmut2 gene[31] were cloned into the pET-Duet-1 vector, replacing genetic elements of the pET vector required for protein overexpression. Mutations were introduced by the QuikChange Site-directed Mutagenesis protocol (Stratagene). The *E. coli* TOP10 cells (Invitrogen) transformed with plasmids were used for the experiments.[19] Colonies were cultured overnight in the LB media supplemented with 100 μg/mL ampicillin. Then, cultures were diluted and grown in the LB media at

37°C for one hour, until OD_{595} reached approximately 0.3. Cells were transferred to 96-well black plates and transparent plates (SPL Life Sciences) for fluorescence and absorbance measurements, respectively, and a final concentration of 3% (v/v) ethanol or MHQ in ethanol was added. The fluorescence of was monitored using the Victor X2 device (Perkin-Elmer) at excitation/emission wavelengths of 485/535 nm, respectively, and the absorbance was measured using the Emax microplate reader (Molecular Devices) at one-hour intervals for 10 hours. Fluorescence was normalized by dividing RFU into OD_{595}, and a response ratio was calculated as follows.[16]

$$response\ ratio = \frac{RFU(MHQ)/OD_{595}(MHQ)}{RFU(ethanol)/OD_{595}(ethanol)}$$

QUANTIFICATION AND STATISTICAL ANALYSIS

Crystallography

Structures were analyzed by using the CCP4[26] and Phenix[29] suites.

Microscale thermophoresis assay

The data analysis was performed using the MO.Affinity Analysis software (NanoTemper Technologies) and OriginPro (OriginLab). Kd's in Table 2 are represented as the mean and standard deviation for 3-4 independent experiments. Error bars in Figure S3 represent the standard deviation of the mean for 3-4 independent experiments.

GFP-based *in vivo* activity assay

Fluorescence data were analyzed as indicated in the method details. Error bars in Figure 6 represent the standard deviation of the mean for 3-4 independent experiments.